# Morphological Evolution of Coherent Misfitting Precipitates in Anisotropic Elastic Media

A. Maheshwari and A. J. Ardell
*Department of Materials Science and Engineering, University of California, Los Angeles, California 90024-1595*
(Received 3 December 1992)

The shapes of coherent misfitting $Ni_3Al$ precipitates were systematically investigated using a parameter $\zeta$ defined essentially by the ratio of particle sizes along $\langle 100 \rangle$ and $\langle 110 \rangle$. The variation of $\zeta$ with size was measured in several alloys using electron microscopy. $\zeta$ does not depend uniquely on particle size; it is also strongly influenced by the volume fraction of $Ni_3Al$. These results provide the first quantitative evidence that elastic interaction energy plays a major role not only in spatial correlations, but also in the morphological evolution of individual particles.

PACS numbers: 64.80.Gd, 81.30.Mh, 81.35.+k

There has been considerable recent interest in the materials physics of morphological evolution and pattern formation during solid-solid phase transformations [1,2]. Such changes are exemplified in Ni-base alloys by the behavior during Ostwald ripening of ordered coherent misfitting precipitates with the composition $Ni_3X$ ($\gamma'$ precipitates). The shape of an individual particle in these alloys is dictated by the elastic self-energy, which is proportional to the volume of the particle and the square of the lattice mismatch, $\varepsilon = (a_p - a_m)/a_m = \Delta a/a$ ($a_p$ and $a_m$ are the lattice constants of the precipitate and matrix phases, respectively). When $|\varepsilon| > 0$ the morphology of $\gamma'$ precipitates evolves from spherical to cuboidal [3] (cubes with faces parallel to $\langle 100 \rangle$ and rounded corners) to concave cuboids [4], which eventually split or bifurcate into plates or octets as their volume increases [5–7]. When $\varepsilon \approx 0$ the particles remain spherical at all sizes [6]. The lattice mismatch is also ultimately responsible for strong spatial correlations during coarsening. These correlations arise through elastic interaction energy, and significantly influence the microstructure of aged Ni-base alloys, leading to dramatic alignment of $\gamma'$ precipitates along elastically soft $\langle 100 \rangle$ directions [3].

The involvement of elastic energy in the evolution of the morphology and spatial distribution of precipitates has been intensively investigated theoretically. The shapes of isolated particles [8], including those characteristic of $\gamma'$ precipitates [9–11], have been predicted by calculating the specific morphologies that minimize the sum of the elastic and interfacial free energies. Voorhees and co-workers [12] have studied the problem of two particles coarsening under the influence of their mutual stress fields. They predict that changes should occur in the morphology of initially spherical particles, although details of the evolving shapes are not specified. Even in the absence of an internal stress spatial diffusional correlations [13] can theoretically affect morphology [14], though the effect is small.

While the theories cited [8–12] demonstrate the influence of elastic energy on morphology, their predictions cannot be applied to real systems because the shapes considered are not in thermodynamic equilibrium. Voorhees, McFadden, and Johnson [15] have recently investigated the thermodynamic equilibrium shapes of an isolated two-dimensional precipitate in an elastically anisotropic matrix as a function of $\varepsilon$ and interfacial free energy. Using physical parameters representative of Ni-base alloys, they found that the particles acquire flattened interfaces along the elastically soft $\langle 01 \rangle$ directions, comparable to what is observed experimentally in real Ni-base alloys along the elastically soft $\langle 001 \rangle$ directions. The role of the volume fraction of particles in morphological evolution, however, has not yet been investigated.

In other recent theoretical advances, Nishimori and Onuki [2] and Wang, Chen, and Khachaturyan [16–18] have used computer simulation to study the evolution of morphology and spatial correlations (pattern formation) in two-dimensional systems of elastically misfitting domains. Their approaches are equivalent to solving a diffusion equation of the Cahn-Hilliard type or a Ginzburg-Landau type in which the effect of elasticity is incorporated. The shapes and spatial arrangements predicted are therefore consistent with the requirements of thermodynamic equilibrium, and the similarities between the simulated and experimentally observed microstructures are remarkable.

We recently reported the results of experiments on the coarsening behavior of $Ni_3Al$ precipitates in aged Ni-Al alloys containing much smaller $\gamma'$ volume fractions $f_{\gamma'}$ than are generally found in such alloys [19]. The reported magnitudes of $\varepsilon$ in this system range from 0.0039 to 0.0057 [20]. In addition to unexpectedly anomalous coarsening behavior [19], we concluded by qualitative examination of the microstructure [4] that the morphological evolution of the $\gamma'$ particles depends on $f_{\gamma'}$. This means that the morphology of $\gamma'$ precipitates at different $f_{\gamma'}$ is dictated not only by the size of an individual particle, but also by its proximity to neighboring particles. The clear implication here is that elastic interaction energy plays a pivotal role not only in the spatial arrangement (pattern formation), but also on the morphology of the particles. This latter finding is not predicted by the theories of morphological evolution of isolated precipitates, or by those that invoke elastic interactions among a

 

few particles, because the role of $f_{\gamma'}$ is precluded. Simulations such as those of Nishimori and Onuki [2] and Wang, Chen, and Khachaturyan [16–18] are in principle capable of exploring this issue, but they have so far been limited to two dimensions and the effect of $f_{\gamma'}$ has not yet been specifically addressed.

The purpose of this paper is to demonstrate quantitatively and conclusively for the first time that the morphological evolution of the shapes of coherent $Ni_3Al$ particles in Ni-Al alloys is a function not only of their average size but also of their volume fraction. We introduce a shape parameter $\zeta$ to quantify the morphology as observed in dark-field transmission electron micrographs of thin foils oriented [001]. $\zeta$ is defined as $a/d$, where $a$ represents the conventionally measured size along $\langle 100 \rangle$ and $d$ is the size measured along a face diagonal. The geometry is depicted schematically in Fig. 1, which also illustrates that $d$ is defined as the size along $\langle 110 \rangle$ when the particles are ellipsoidal and their projected images are ellipses. The value of $\zeta$ lies in the range $1 < \zeta < \sqrt{2}/2$ so long as the morphology is cuboidal, varying from perfect spheres ($\zeta = 1$) to perfect cubes ($\zeta = \sqrt{2}/2$). However, $\zeta$ can be smaller than $\sqrt{2}/2$ when the interfaces of the cuboids are concave [4], and greater than unity when the particles are ellipsoidal.

Measurements of $\zeta$ were made on enlarged dark-field micrographs using a digitizer. The contrast of the images in positive prints, the inherent accuracy of the digitizer tablet, and uncertainties in the precise locations of the interfaces are the greatest sources of error, which are much larger for small particles ($a \sim 10$ nm) than for large ones ($a > 50$ nm). The average value of the two edge distances, $a_1$ and $a_2$, along [100] and [010], and the corresponding average values of $d_1$ and $d_2$, were measured for individual particles in alloys containing from 5.72 to 6.35

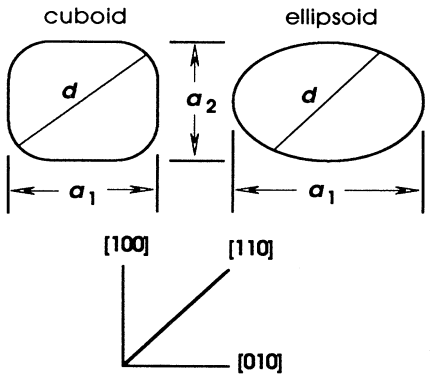


FIG. 1. Schematic drawing illustrating the measurement of $\zeta$. The cuboidal particle on the left has been deliberately drawn nonequiaxed to show how $d$ is determined (it is not necessarily parallel to $\langle 110 \rangle$). For ellipsoidal particles, i.e., when there is no interface obviously parallel to $\langle 100 \rangle$, $d$ is measured along $\langle 110 \rangle$. The values of $a$ and $d$ for individual particles are taken as $(a_1+a_2)/2$ and $(d_1+d_2)/2$.

TABLE I. Alloy compositions, $\gamma'$ volume fractions, $f_{\gamma'}$, and ranges of particle sizes, $a_{min} < a < a_{max}$ (nm).

| wt.% Al | $f_{\gamma'}$ | $a_{min}$ | $a_{max}$ |
|---|---|---|---|
| 5.72 | 0.025 | 22.3 | 108.9 |
| 5.78 | 0.034 | 11.2 | 107.8 |
| 6.35 | 0.130 | 7.6 | 26.1 |

wt.% Al aged at 630 °C. The compositions, ranges of average particle sizes, and equilibrium values of $f_{\gamma'}$ for the data reported herein [21] are presented in Table I. Only particles for which $0.8 < a_1/a_2 < 1.2$ were included in the analysis. This ensures the exclusion of particles with extreme shapes such as plates or rods.

Representative dark-field electron micrographs illustrating the morphology of the $\gamma'$ precipitates in two specimens with comparable average sizes ($\sim 17$ nm), but for which $f_{\gamma'} = 0.034$ and 0.130, are shown in Fig. 2. The shapes of the particles in Fig. 2(a) are generally more cuboidal than those in Fig. 2(b), consistent with the qualitative observations previously reported [4]. Quantitatively, the effect of $f_{\gamma'}$ is clearly demonstrated by comparing the dependences of $\bar{\zeta}$ with $\bar{a}$ for these two microstructures in Fig. 3. In Fig. 3 $\bar{\zeta}$ represents the average value of $\zeta$ lying in an interval $\Delta a$ within which $\bar{a}$ is the average value of $a$. The error bars in Fig. 3 reflect the standard deviations of $a$ and $\zeta$ in each interval. The standard deviation of $\zeta$ exceeds unity in some cases because there are small particles in Fig. 2(a) which project as ellipses, as predicted by the computer simulations of Wang, Chen, and Khachaturyan [17]; these contribute values of $\zeta > 1$ to the statistics. It is evident in Fig. 3 that the values of $\bar{\zeta}$ for $f_{\gamma'} = 0.034$ are significantly smaller than those for $f_{\gamma'} = 0.130$. This means that the morphology of the particles evolves from spheres to cuboids more readily as the supersaturation is reduced.

The variation of $\bar{\zeta}$ with $\bar{a}$ in the alloys with $f_{\gamma'} = 0.025$ and 0.034, over the entire range of $a$ investigated, is shown in Fig. 4. It is apparent that when $f_{\gamma'} = 0.025$ almost all the particles attain a value of $\bar{\zeta}$ less than $\sqrt{2}/2$ even when $\bar{\zeta} < 25$ nm; nearly all the precipitates are concave cuboidal [4]. In the alloy with $f_{\gamma'} = 0.034$ the evolution from spheres to cuboids was very rapid, $\bar{\zeta}$ decreasing from about unity to $\approx 0.75$ within a few tens of nanometers, the shape nearly stabilizing after this rapid decrease. From the trends seen in Figs. 3 and 4, it appears that the larger $f_{\gamma'}$ is the slower the evolution of the morphology, but this observation awaits more data before it can be deemed conclusive.

The results presented herein support the idea that the morphological evolution of individual particles is strongly influenced by elastic interactions. However, it is important to consider the possibility that the concave cuboidal shape, in particular, is a consequence of preferential dendritic growth at the corners of the cuboidal particles, as suggested by the recent observations of Yoon and co-

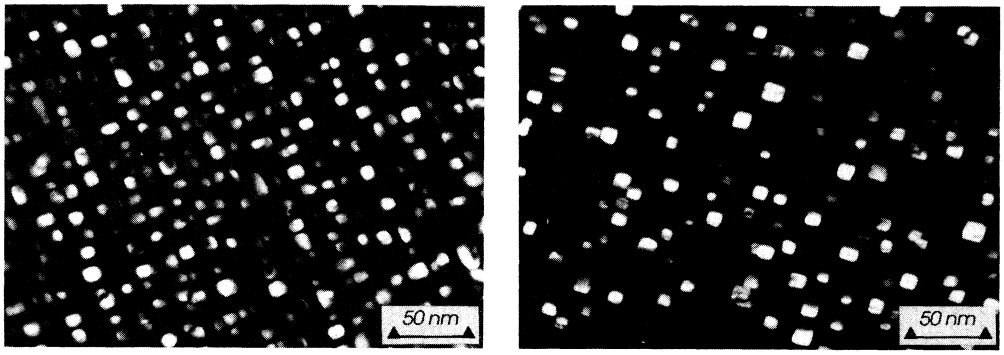


FIG. 2. Dark-field transmission electron micrographs taken using (100) $\gamma'$ precipitate superlattice reflections: (a) 6.35 wt.% Al aged for 92.5 h, $f_{\gamma'}=0.130$; (b) 5.78 wt.% Al aged for 54 h, $f_{\gamma'}=0.034$. The average precipitate size for the entire population of precipitates under the aging conditions in (a) is 17.3 nm. For the aging conditions in (b) it is =16.4 nm.

workers [22]. They observed similar $\gamma'$ precipitate morphologies in Ni-base alloys aged at small supersaturations. Dendritic growth by the mechanism of Mullins and Sekerka [23] occurs when a perturbation of radius $r$ exceeds a critical value $r_c$ given by

$$r_c = \frac{14\sigma\Omega}{RT[\Delta c/c_e]}, \tag{1}$$

where $\Delta c/c_e=(c-c_e)/c_e$ is the supersaturation when the far-field and equilibrium solute concentrations are $c$ and $c_e$, respectively, $\sigma$ is the free energy of the precipitate-matrix interface, $\Omega$ is the molar volume of the precipitate phase, $R$ is the gas constant, and $T$ is the absolute temperature. For our alloy containing $f_{\gamma'}=0.025$, $r_c$ can be estimated using $\sigma=14$ mJ/m$^2$ and $\Omega=27.16\times10^{-6}$ m$^3$/mol from earlier work [24], and the maximum value of $\Delta c/c_e$ based on the measured solubility limit [19]. With $\Delta c/c_e=0.0152$, we find $r_c\approx47$ nm as the minimum value of this parameter in our experiments. Since $2r_c$ is comparable in size to the largest of the precipitates in our alloy (Fig. 4), we conclude that dendritic growth is improbable under the small supersaturations characteristic of our experiments.

It thus follows that all the morphologies observed evolve during coarsening. This conclusion is further supported by several other observations. First, the number of $\gamma'$ precipitates per unit volume $N_v$ in all the alloys we examined decreased with aging time. $N_v$ would be approximately constant if the excess supersaturation were being depleted by dendritic growth. Second, in the alloy containing $f_{\gamma'}=0.025$, some of the smaller-than-average particles in the particle size distributions were concave cuboids, suggesting that at least some particles retain this morphology even while *dissolving*. Furthermore, since precipitates of near average size are neither growing nor shrinking, they would equilibrate to a more stable morphology if there were some driving force to do so. This is

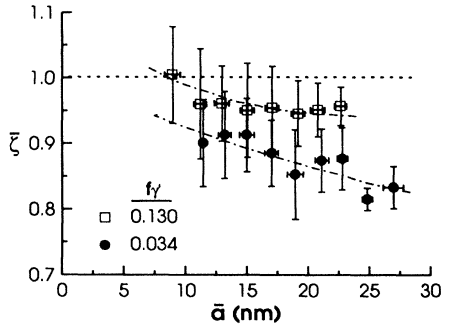


FIG. 3. The variation of $\bar{\zeta}$ with $\bar{a}$ over the range 10 to 30 nm for the alloys containing 6.35 and 5.78 wt.% Al ($f_{\gamma'}=0.130$ and 0.034, respectively). $\bar{\zeta}$ and $\bar{a}$ were computed for intervals $\Delta a=2$ nm. The horizontal line at $\bar{\zeta}=1$ represents the limit of $\zeta$ for perfect spheres. The dash-dotted curves are drawn to indicate the trends in the data.

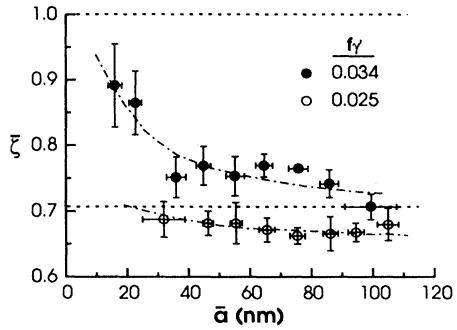


FIG. 4. Illustrating the variation of $\bar{\zeta}$ with $\bar{a}$ for the alloys containing 5.78 and 5.72 wt.% Al ($f_{\gamma'}=0.034$ and 0.025, respectively). The averages in this case were computed from data lying within intervals of $\Delta a$ equal to or exceeding 10 nm, which is why all the data for $f_{\gamma'}=0.034$ in Fig. 3 are represented by only two points here. The horizontal lines at $\bar{\zeta}=1$ and 0.717 represent the limits of $\zeta$ for perfect spheres and cubes, respectively. The dash-dotted curves are drawn to indicate the trends in the data.

because the diffusion distances involved in transporting atoms from the corners to the face centers of the cuboids are much smaller than the diffusion distances during growth or coarsening, especially when $f_{\gamma'}$ is so small. Last, concave-cuboidal $Ni_3Al$ precipitates are plainly visible in Fig. 1 of the early paper of Miyazaki, Imamura, and Kozakai [5], who observed the subsequent splitting of these precipitates into parallel plates with increased aging time, as opposed to continued dendritic corner growth. They were careful to age their alloy under conditions of Ostwald ripening.

It is perhaps not surprising that elastic interactions influence morphology in view of the early observation [3] that the stress fields of dislocations strongly affect the morphology, size, and spatial distribution of $\gamma'$ precipitates in aged Ni-Al alloys. Additionally, externally applied stresses are also expected to influence the morphological evolution of coherent particles [25]. It is therefore reasonable to anticipate that internal stresses generated by neighboring precipitates will affect the shapes of individual ones, as well as the spatial correlations leading to pattern formation in elastically anisotropic materials. The role of other factors in this process, such as differences between the elastic constants of the $\gamma'$ and matrix phases, has not been clarified. Experiments designed to systematically explore the dependence of morphological evolution of $\gamma'$ precipitates on $f_{\gamma'}$ in Ni-Si, Ni-Ga, and Ni-Ge alloys, all of which are characterized by different values of $\varepsilon$ and elastic constants, are currently in progress.

Financial support from the National Science Foundation under Grant No. DMR-8901555 is gratefully acknowledged.

[1] R. Toral, A. Chakrabarti, and J. D. Gunton, Phys. Rev. B **39**, 901 (1989).
[2] H. Nishimori and A. Onuki, Phys. Rev. B **42**, 980 (1990).
[3] A. J. Ardell and R. B. Nicholson, Acta Metall. **14**, 1295 (1966).
[4] A. Maheshwari and A. J. Ardell, Scr. Metall. Mater. **26**, 347 (1992).
[5] T. Miyazaki, H. Imamura, and T. Kozakai, Mater. Sci. Eng. **54**, 9 (1982).
[6] M. Doi, T. Miyazaki, and T. Wakatsuki, Mater. Sci. Eng. **67**, 247 (1984).
[7] M. J. Kaufman, P. W. Voorhees, W. C. Johnson, and F. S. Biancaniello, Metall. Trans. A **20**, 2171 (1989).
[8] W. C. Johnson and J. W. Cahn, Acta Metall. **32**, 1925 (1984).
[9] T. Miyazaki, K. Seki, M. Doi, and T. Kozakai, Mater. Sci. Eng. **77**, 125 (1986).
[10] A. G. Khachaturyan, S. V. Semenovskaya, and J. W. Morris, Jr., Acta Metall. **36**, 1563 (1988).
[11] M. T. McCormack, A. G. Khachaturyan, and J. W. Morris, Jr., Acta Metall. Mater. **40**, 325 (1992).
[12] P. W. Voorhees and W. C. Johnson, Phys. Rev. Lett. **61**, 2225 (1988); W. C. Johnson, P. W. Voorhees, and D. E. Zupon, Metall. Trans. A **20**, 1175 (1989); W. C. Johnson, T. A. Abinandan, and P. W. Voorhees, Acta Metall. Mater. **38**, 1349 (1990).
[13] M. Marder, Phys. Rev. Lett. **55**, 2953 (1985); Phys. Rev. A **33**, 4482 (1987).
[14] T. Imaeda and K. Kawasaki, Physica (Amsterdam) **164A**, 335 (1990); **186A**, 359 (1992).
[15] P. W. Voorhees, G. B. McFadden, and W. C. Johnson, Acta Metall. Mater. **40**, 2979 (1992).
[16] Y. Wang, L. Q. Chen, and A. G. Khachaturyan, Scr. Metall. Mater. **25**, 1387 (1991).
[17] Y. Wang, L. Q. Chen, and A. G. Khachaturyan, Scr. Metall. Mater. **25**, 1969 (1991).
[18] Y. Wang, L. Q. Chen, and A. G. Khachaturyan, Phys. Rev. B **46**, 11 194 (1992).
[19] A. Maheshwari and A. J. Ardell, Acta Metall. Mater. **40**, 2661 (1992). The coarsening behavior is anomalous in that the rates decrease with increasing $f_{\gamma'}$.
[20] E. Hornbogen and M. Roth, Z. Met. **58**, 842 (1967); V. A. Phillips, Philos. Mag. **16**, 103 (1967); E. Nembach and G. Neite, Prog. Mater. Sci. **29**, 177 (1985).
[21] The values of $f_{\gamma'}$ in Table I differ slightly from those in Ref. [18] because the small correction for the different mass densities of the matrix and precipitate phases has been taken into account.
[22] D. Y. Yoon, M. F. Henry, S. J. Yeom, and Y. S. Yoo (unpublished). Brief descriptions of their findings are presented in Proceedings of the 1992 MRS Meeting and Proceedings of the 1992 TMS Annual Meeting Abstract Bulletins (unpublished).
[23] W. W. Mullins and R. F. Sekerka, J. Appl. Phys. **34**, 323 (1963).
[24] A. J. Ardell, Acta Metall. **16**, 511 (1968).
[25] W. C. Johnson, Metall. Trans. A **18**, 233 (1987); W. C. Johnson, M. B. Berkenpas, and D. E. Laughlin, Acta Metall. **36**, 3149 (1988).

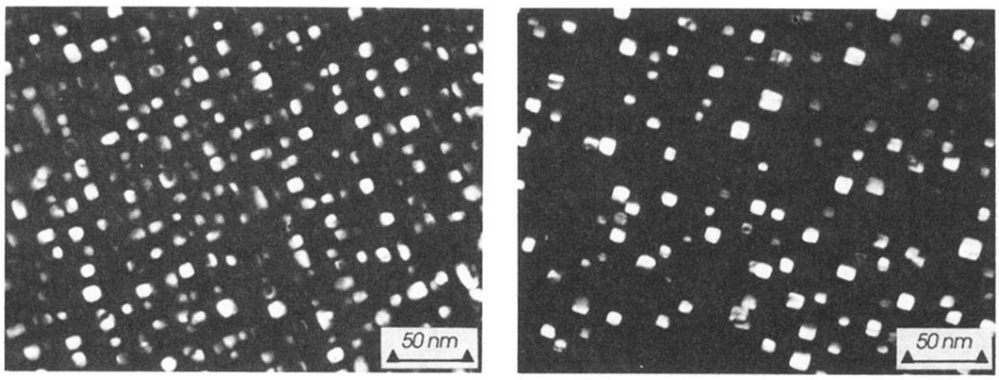


(a) (b)

FIG. 2. Dark-field transmission electron micrographs taken using (100) $\gamma'$ precipitate superlattice reflections: (a) 6.35 wt.% Al aged for 92.5 h, $f_{\gamma'}=0.130$; (b) 5.78 wt.% Al aged for 54 h, $f_{\gamma'}=0.034$. The average precipitate size for the entire population of precipitates under the aging conditions in (a) is 17.3 nm. For the aging conditions in (b) it is $=16.4$ nm.